Adsorption of Scandium and Yttrium from Aqueous Solutions by Purolite C100Na Resin: Equilibrium and Kinetic Modeling

Hajmohammadi, Hamid; Jafari, Abdol Hamid*[+]

Department of Metallurgy and Materials Science, Shahid Bahonar University of Kerman, I.R. IRAN

Eskandari Nasab, M

Mineral Processing Engineering, Zarand College, Shahid Bahonar University of Kerman, Zarand, I.R. IRAN

ABSTRACT: *Adsorption of Sc from single and bi-component Sc-Y solutions by Purolite C100Na was studied experimentally and kinetic and thermodynamic characteristics are described. The extended Freundlich isotherm was found to be successful in validating the experimental results. Moreover, the curve fitting the time-dependent data into different kinetics mechanisms showed a satisfactory correlation with the pseudo-second-order model. Binary system results show a decrease in Sc adsorption capacity of the absorbent in presence of secondary ions due to competition for adsorption sites. Furthermore, thermodynamic parameters indicate similarity of reaction mechanisms for both single and binary systems, with Sc absorption adversely affected by temperature. Results from synthetic solutions with an actual Y/Sc ratio of 5 were used for extracting scandium from actual mining copper leach solution by circulating it through a resin column. The results demonstrate a satisfactory collection of Sc ions despite the fivefold concentration of Y over Sc. The elusion studies showed that the yttrium desorption peak occurs before that of Sc which corroborates the adsorption isotherm findings. This results in a 180 mg/L Sc rich solution or 60:1 concentration ratio over the original copper leach solution.*

KEYWORDS: *Scandium; Yttrium; Adsorption; Ion exchange; Thermodynamic isotherm; Purolite C100.*

INTRODUCTION

The term "rare earths" denotes seventeen chemically similar metallic elements, That include scandium, yttrium, and the lanthanides[1] among which Sc is the most expensive with a variety of uses in nuclear technology, aerospace and airplane production, electronics, ceramic catalysts and metal halide lamps [2-4]. Sc use is also growing in solid fuel cells because of the high oxygen ion conductivity of Sc_2O_3-stabilized-ZrO_2 solid electrolytes even at lower temperatures [5] and recently, it has been used to enhance the piezoelectric response in aluminum

***** *To whom correspondence should be addressed.*
+ E-mail: Jafari.a.h@uk.ac.ir
1021-9986/2021/4/1132-1147 16/$/6.06

nitride alloys [6]. The annual world production of Sc is 10-15 tons but due to limited supply and growing demand the price is steadily increasing [7]. Although scandium is found in more than 100 natural minerals, ores containing economical assays for mining operations are extremely rare [8, 9], thus, it is always extracted from by-products of other mining and metal smelting processes. These include U, W, Nb, Ti, Ta, Ni, and Al refining treatments [10,11]. To understand the rarity of this element suffice it to say that in Australia, uranium wastewater from uranium leach extraction with only one ppm Sc is used as a primary source, while the U.S. producers have to take uranium solutions with as little as 0.6 ppm [11-13]. Leaching of copper ores is routinely done in many mines to make use of copper oxide deposits. During the operation, sulfuric acid reacts with the ores and releases various cations including the multitude of rare earth metals. The electrowinning technique is then employed for separating copper which leaves other constituents untouched [14, 15]. Copper leach solutions in the Iranian Sarcheshmeh Copper mines, regularly contain 3 ppm Sc and 15 ppm of Y without the concern for radioactivity associated with U-leach waste and yet to date, apart from a number of research done on recovery of other rare earth metals, [14, 15], no research is published for removal of this important element. The methods for rare earth metal extraction usually comprise pre-concentration, separation, and adsorption stages [16]. The latter stage could include solvent extraction, ionic liquids, solvent impregnated resins, active carbon, nano-size oxides, graphene oxide although some very exotic reagents are also reported such as pineapple crown, grapefruit peel, crab shell, saw-dust bone powder [17-23]. Solvent extraction has inherent problems such as liquid evaporation, miscibility of organic and aqueous phases, flammability of compounds, toxicity, and general environmental pollution [2,24]. Ionic liquids, a variant of this technique claims certain improvements such as low evaporation pressure of the constituents, inflammability, and temperature stability [25], however, these are not proven in practice on a commercial scale and many are not verified to be non-toxic and totally safe in long-duration use to grant labeling as a "green" technique [26,27]. Furthermore, the main obstacle facing the commercialization of such techniques is their effectiveness only in high concentrations of the adsorbate [28]. Ion exchange, is a reversible ionic reaction between a solid and a liquid phase without alteration of adsorbent structure [29-32] and rare earth elements are generally extracted by ion exchange technique or solvent extraction [33,34]. Due to the high surface available and the ease of operation, the economical extraction of low-grade elements such as Sc is only viable by ion-exchange columns [35]. A case in point is Australian commercial recovery of ion Sc from 1 ppm Sc uranium leach solution through exchange technique [11, 12]. A problem with ion exchange recovery of rare earth metals, in general, is the lack of chelating resins for them and so their scavenging must be done using strong cationic resins [16,36]. *Broekaert et.al.* (1981) [37], *Ochsenkuhn et.al.*(2002) [30], *Page et.al.*(2017) [29], and *Felipe et.al.* (2020) [16] report using Dowex 50W-X8 for the lanthanides extraction from HCl electrolyte in the 0.1-10 ppm concentration range, Sc scavenging from red mud dissolved in hydrochloric acid, and rare earth elements from uranium leach solution and U-mine waters. *Koopman et.al.* (1999) [38] studied Purolite C 100 for rare earth elements extraction from phosphoric acid medium and *Petropoulou et.al.*(2002) [30] employed it for Sc recovery from red mud produced during Al making dissolved in nitric acid. *Alexey et.al.* (2017) [36] describe the use of strong acid resins; Purolite D 5041, Tulsion CH 93, Lewatit TP 260, Purolite S 950 for Sc recovery from uranium leach solutions. *Chour et.al* (2018) [39], report the result of applying strong acid resin AMBERLITE™ IRN77 H and Purolite C 160 to recover rare earth elements from nitrite solutions.

Purolite C 100 as a strong acid polymer is capable of adsorbing various cations [11, 29, 30], and its behavior for interacting with Ca, Ce, Pb, Fe, Gd is reported [40,41], Kinetics and thermodynamics of heavy metals' adsorption are studied for determining the mechanism, the adsorbent capacity and diffusion steps involved [42-44], however, its adsorption thermodynamic and kinetics especially in presence of other cations which could cause synergism, antagonism, or non-interaction, are not studied. *Langeroodi et.al.* (2018) [45] studying iron adsorption from aqueous solutions by metallic nano-composites establish Langmuir isotherm for the adsorption and pseudo-second-order for its kinetics. *Safaei et.al.* (2019) [46] report Cu adsorption using carbon black and find the same kinetics mechanism. *Langeroodi et.al.*(2019), [47] employed a mixture of wheat bran and Japanese medlar core-shell for Mn scavenging and noted the adsorption

model as Langmuir isotherm. *Dubey* and *Grandhi* (2016) [23], find the adsorption mechanism of Y from aqueous solutions by nano maghemite follows the Langmuir isotherm and its kinetics is governed by a pseudo-second-order mechanism. *Burakova et.al.* (2018), [17] and *Bao et.al.* (2018), [48] using active carbon and exchange resins TP 209، TP 260 and TP 272 for Sc adsorption from sulfate environment report similar kinetics mechanism. Chemically due to the close ion radii, Sc functions similar to Al, Y, and lanthanides in general, and in nature, they are found together [49], and thus these elements in multi-component systems could be absorbed concurrently by the resin [29,30]. The present study concentrates on adsorption of Y and Sc on Purolite C100Na, a strong acid gel-type resin either individually or together both in static (batch) or dynamic (continuous) modes for establishing the mechanisms involved and by optimizing them establish a way for applying this technique to Sc separation from copper acid leach solution from actual mining operations.

EXPERIMENTAL SECTION

Materials and reagents

All reagents were of analytical grade and used without further purification. Stock solutions containing Sc and Y were prepared by dissolving $Sc(NO3)_3.xH_2O$ and $YCl_3.6H_2O$ procured from Aldrich, in double-distilled water and the pH was regulated at 1.5 and at the reported temperature range while being continuously agitated in an incubator shaker (Innova 4200). Sulfuric acid and Nitric acid from Merck were used to make the elusion solutions. Purolite C100 from Purolite Co. with the physical and chemical properties shown in Table 1 was used. The concentration of metal ions in solutions was determined before and after each test using ICP-OES (VARIAN 735-Es) machine. FE-SEM device model Sigma VP, ZEISS, equipped with EDS detector was used to study the structure and distribution of Sc and Y elements on the surface and inside of resin nodules which were fractured in liquid nitrogen after the sorption process. FT-IR analysis of the adsorption/desorption behavior was done using a NEXUS TM 470FT-IR ESP unit. The final step consisted of experiments on the actual copper leach solution of the composition Table 2 and pH=1.5, by passing it through a column containing 20 mL of resin at 100 mL/h.

Table 1: Physical and chemical properties of Purolite C100 ion exchange resin.

Property	Description
Basic information	
Structure	Gel type
Matrix	Polystryrene/divinylbenzene
Functional group	Sulfonic
Ionic form	Na^+
Physical/chemical	
Bead size	0.3–1.2 mm
Specific gravity	1.29 (in Na^+ form)
Moisture retention	44–48% (in Na^+ form)
Total capacity	2 meq/mL

Table 2: Chemical Composition of Copper Raffinate Leach Solution.

Element	Sc	Y	Ce	Al	Fe	Cu
Concentration (mg/L)	3.2	14.9	2.6	8037	6034	153

Experimental Method

Resin treatment

Immersing resin beads in de-ionized water for 20 min removes impurities and helps open up the pores and cavities to enhance the adsorption process. The beaker containing 20 g of resin is five times the resin volume de-ionized water was stirred by a magnetic shaker for 15 min until the resin pearls are precipitated, and then the water was drained. This step was repeated five times and the final filtered pearls were dried in an oven at 50 ° C for 24 hours. The dried resin is collected in a capped plastic container and placed in a desiccator until the time it was used in experiments.

Experimental procedure

Kinetics and thermodynamics investigation of adsorption phenomenon was carried out on electrolytes containing single and binary ions at specific temperatures of 298, 308, 318, and 328K. For single ion solutions, in 200 mL flasks, about 0.1 g of resins pearls were mixed with 50 mL of 150 to 500 ppm ion concentration solutions. The efficiency of ion adsorption was determined from the difference between the initial and final Sc concentration in the solution [43]. To simulate conditions

in the copper refinery in Sarcheshmeh copper mine, Sc concentration was altered within the bath's actual range of 60 to 100 ppm but the concentration of Y was adjusted for the Y to Sc ratio of 5 which is the norm in the actual copper leach solution. A thermostatic shaker continuously stirred flasks for 24 h at 130 rpm to reach the equilibrium state. Double ion tests were performed using 0.1 g of the adsorbent in 50 mL solution but this time the electrolyte carried 100 mg/L Sc and 500 mg/L Y together. The capacity of adsorbed metal was calculated from the mass balance equation as follows:

$$q_e = \frac{C_0 - C_e}{W} V \quad (1)$$

Where C_0 and C_e, are metal ion concentrations (mg/L) at the beginning and after attaining equilibrium, V, is the total volume of solution (L) and W is the weight of dry resins (g) [36]. Adsorption characteristics of the resin were further investigated from FT-IR studies on single and double ion solutions before and after adsorption.

RESULTS AND DISCUSSION

Adsorption isotherms

Adsorption isotherms at constant temperature are important to obtain equilibrium parameters necessary for understanding how atoms, molecules, or ions associatively or dissociative interact with sorbent sites, allowing to predict the extent to the adsorbate and adsorbent interact [44]. Such studies assist in optimizing adsorption systems and estimating the adsorbent capacity by better understanding the adsorption process [43].

While analyses of adsorption from single constituent systems can give a lot of valuable information, evidently, it cannot determine the nature of equilibrium interactions in multi-component systems due to the complicated relations between various ions and adsorbents [50]. To assess the effects of the competitive adsorption on Sc uptake by the adsorbent, in presence of Yttrium, thermodynamic, kinetic, and adsorption mechanisms from acid solutions with Sc and Y alone and then binary Sc-Y, electrolytes were investigated.

Adsorption isotherms for single-component systems

Equilibrium adsorption data from experiments on Sc and Y laced in synthesized solutions once individually and then jointly are used for determining the isotherm model governing the adsorption processes. Four of the most frequently applied isotherm models (Eqs.(2–5)), Langmuir, Freundlich, Temkin, and Dubinin–Radushkevich (D-R) [43] are considered. The calculated isotherm parameters are listed in Table 3.

$$\text{Langmuir}: \frac{C_e}{q_e} = \frac{C_e}{q_{max}} + \frac{1}{q_{max} K_1} \quad (2)$$

$$\text{Freundlich}: \log q_e = \log K_f + \frac{1}{n} \log C_e \quad (3)$$

$$\text{Temkin}: q_e = \frac{RT}{b} \ln A + \frac{RT}{b} \log C_e \quad (4)$$

$$\text{Dubinin} - \text{Radushkevich (D-R)}: \quad (5)$$

$$\ln q_e = \ln q_m - \beta \left[RT \ln \left(1 + \frac{1}{C_e} \right) \right], \quad E = \frac{1}{\sqrt{2\beta}}$$

q_e is the equilibrium amount of metal adsorbed on the resin (mg/g), C_e is the equilibrium metal ion concentration in solution (mg/L), q_{max} is the monolayer maximum ion capacity of the resin (mg/g), K_l and K_f are the Langmuir and Freundlich constants respectively related to the energy of adsorption (L/mg), $1/n$ is the heterogeneity factor, A and b the Temkin constants, q_m the Dubinin-Radushkevich monolayer capacity (mg/g) and β (mol^2/kJ^2) a constant with dimensions of energy, and E is the mean free energy of adsorption per mole of the adsorbate (kJ/mol).

As the results in Table 3 show, high R^2 values for the linear juxtaposition of data from single-component adsorption experiments, and the Freundlich isotherm is the model best-describing adsorption from this electrolyte irrespective of whether Scandium or Yttrium is being studied.

In this model, the "n" value is inversely proportional with the affinity of the adsorbent sites for the ion being investigated and should fall between 1<n<10 if the adsorbent is to be classification as effectual [51]. According to Table 3, n values for both elements fall in the 1 to 10 range, indicating the proficiency of the adsorbent and ease of absorption of that ion from the solution. The higher n values calculated for Y indicate the intense heterogeneity of the adsorbent surface for the ions of this metal compared to scandium.

The characteristic of the Langmuir model is its assumption that no interaction between the absorbent and the adsorbate ions exist and furthermore the active adsorbent sites are homogenously distributed, thus, adsorption is assumed to

Table 3: Isotherm constants for different models for SC and Y adsorption on Purolite C100 from single component system.

Isotherm	Constants	Sc	Y
Langmuir	q_{max} (mg/g)	98.03±0.01	106.29±2.01
	K_l (L/mg)	8.50±0.84	6.89±0.01
	R^2	0.90	0.89
Freundlich	K_f ((mg/g)/(mg/L)$^{1/n}$)	46.05±2.62	47.31±2.03
	n	6.65±0.27	7.20±0.07
	R^2	0.99	0.94
Temkin	A(L/mg)	3.52±0.28	3.10±0.14
	b(J/mol)	85.79±3.37	55.49±0.31
	R^2	0.98	0.94
D-R	q_m (mg/g)	12.37±0.00	13.69±0.01
	β (mol^2/kJ^2)	$2*10^{-8}$±0.00	$3*10^{-8}$±0.00
	E (kJ/mol)	5.00±0.00	4.08±0.00
	R^2	0.84	0.86

proceed to form a monolayer [52, 53]. Table 3, shows the maximum Langmuir monolayer capacities (q_{max}) for Sc and Y are 98.03 and 106.29 mg g^{-1} respectively. In this model K_l, signifies attractive force of adsorbent for a particular element over the other which according to data is higher for Sc. Temkin isotherm assumes the collective heat of adsorption of ions is a function of the sum of all ion temperatures which decreases linearly rather than logarithmically with coverage excluding the extreme low and high adsorbent concentrations [54]. As Table 3 shows, this model has the highest compliance with empirical data after the Freundlich model. Value of b in this isotherm indicates the energy spent for breaking up the bond between a mole of the absorbent which according to the findings of Table 3 is more for Sc, indicating that, in the process of elution of the resin, yttrium is separated first, and then scandium is removed from the resin.

The D-R model while expressing adsorption mechanisms utilizes the value E to generally characterize the physical or chemical nature of adsorption of metal ions. It is the average energy needed for removal of adsorbed ion species from adsorbate [55] so a low value says, below 8 kJ/mol, specifies the physical adsorption, and if, in the 8–16 kJ/mol range, it denotes chemical adsorption [56-58]. As shown in Table 3, this value for Sc and Y stays below 8 kJ/mol validate the physical nature of the adsorption process. It has been reported that physical adsorption occurs layer upon layer [28,59] and in the present work in order to investigate the nature of Sc adsorption on Purolite, FE-SEM images from the cross-section of the resin beads before and after exposure to the electrolyte, were studied. Fig. 1 shows the high-resolution structure of the adsorbed mass of Sc revealing the stratified makeup corroborating the findings that indicate the adsorption follows Freundlich model. As indicated above, Sc adsorption is best described through Freundlich model supporting stratified adsorption in which the high values of the parameter "n" describe the departure from the homogeneity of the surface adsorption[51]. As the n value for Sc stands at 6.65, then it indicates heterogeneous adsorption. Fig. 1 clearly shows such a heterogeneous layered structure.

Adsorption isotherms for multi-component systems

Multi-component solutions complicate the process by competitive interactions between dissimilar adsorbates attempting to connect to the adsorbent. To illuminate such function, several methods have been developed that derive from the single-component system analysis [50]. Eqs. (6–9) pertain to Extended Langmuir, Modified Langmuir, Extended Freundlich, and Langmuir-Freundlich models which are the most commonly used models for binary-component systems, and thus, they are used to describe the processes involved in the present work.

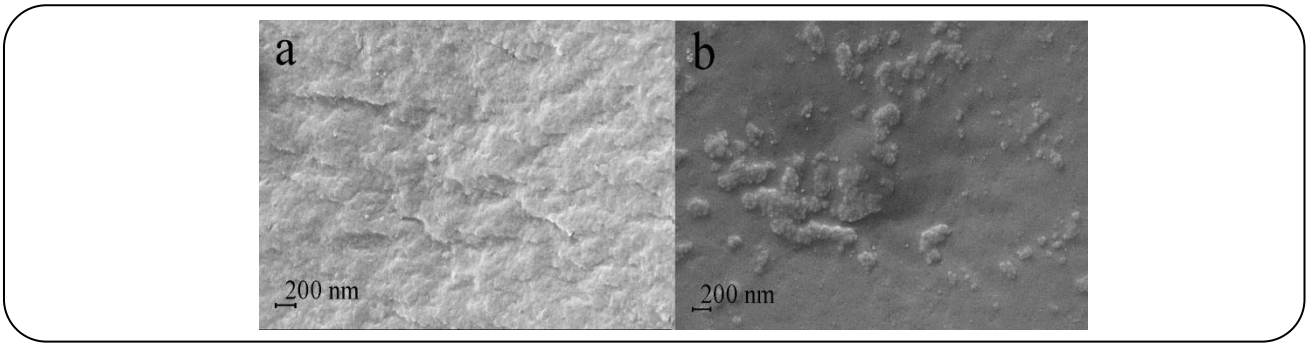

Fig. 1: FESEM pictures from Purolite resin a) Before Sc adsorption b) After Sc adsorption.

$$\text{Extended langmuir}: q_{e,i} = \frac{q_{max} K_{l,i} C_{e,i}}{1 + \sum_{j=1}^{N} K_{l,j} C_{e,i}} \quad (6)$$

$$\text{Modified langmuir}: q_{e,i} = \frac{q_{max,i} K_{l,i} \left(\frac{C_{e,i}}{\eta_i} \right)}{1 + \sum_{j=1}^{N} K_{l,j} \left(\frac{C_{e,i}}{\eta_i} \right)} \quad (7)$$

$$\text{Extended freundlich}: q_{e,i} = \frac{q_{f,i} C_{e,i}^{n_i + x_i}}{\sum_{j=1}^{N} C_{e,i}^{x_i} + y_i C_{e,j}^{z_i}} \quad (8)$$

$$\text{Langmuir} - \text{freundlich}: q_{e,i} = \frac{a_i C_{e,i}^{\frac{1}{m_i}}}{\sum_{j=1}^{N} b_j C_{e,j}^{\frac{1}{m_j}}} \quad (9)$$

$q_{e,i}$ is the equilibrium amount of adsorbed from component *i*, $C_{e,i}$ the equilibrium concentration of component i, $C_{e,j}$ (j = 1, 2, …, N; N is the number of the components) is the equilibrium concentration of each component, $K_{l(i,j)}$ and ($K_{f(i,j)}$,n_i) are the Langmuir and Freundlich constants for component i and j respectively and $q_{max,i}$ is the maximum adsorption capacity for component i. Single adsorption isotherm experiments are used to obtained $q_{max,i}$, n_i and $K_{l,f(i,j)}$. The other parameters ($\eta_{i,j}$, x_i, y_i, z_i, a_i, b_j, $m_{i,j}$) can be found from the curve fitting which was performed in MATLAB program[50]. RMSE (the root of mean square errors) was also used to evaluate the quality of the fitting. RMSE is given as:

$$RMSE = \sqrt{\frac{\sum_{i=1}^{n} \left(X_{obs,i} - X_{model,i} \right)}{n}} \quad (6)$$

Where $X_{obs,i}$ are the observed values and $X_{model,i}$ are the modeled values [43]. The relevant constants, parameters, correlation coefficients (R^2), and RMSE derived from analysis of data from adsorption studies on Purolite resin are given in Table 4. This data shows the Langmuir-Freundlich model with its higher coefficients of determination R^2, and lower RMSE values can be used to describe the Sc-Y binary system in contact with the Purolite adsorbent.

The effect of mutual interaction between metal ions on adsorption capacity can be assessed using the ratio $\frac{q_e^{mix}}{q_e}$ where q_e^{mix} and q_e are the sorption capacity for a particular metal ion in binary and single systems respectively. Three possibilities exist. If $\frac{q_e^{mix}}{q_e} > 1$, synergism of sorption happens i.e. the adsorption of target species will be enhanced in presence of other ions. A $\frac{q_e^{mix}}{q_e} = 1$ indicates no net interaction effect is observed while for $\frac{q_e^{mix}}{q_e} < 1$, antagonistic effect occurs whereby the ion adsorption is less than that of individual adsorbates [60, 61]. Under Sc-Y binary system experimental conditions, the $\frac{q_e^{mix}}{q_e}$ for Sc is 0.23, implying the inhibitory effect of competing Y on the binding of Sc^{+3} to adsorbent vacant sites, and accordingly scandium ions adsorption on Purolite is suppressed in favor of Yttrium. This is not as may be construed as an indication of preference for Y, rather, it shows a concentration effect signifying overcrowding due to the fivefold concentration of Y over Sc. Fig 2 shows FE-SM and elemental map analysis results of sectioned Purolite bead following $Sc^{2+}$and Y^{3+} adsorption from solutions containing these ions individually and combined. The preference of Purolite for Sc in competition for available sites is evident from the rich accumulation of this ion both on the pearls' surface or core, although the abundance of Y ions in the solution

Table 4: Multi-component isotherm parameters for the simultaneous adsorption of Sc and Y on Purolite C100.

Adsorbate	Extended Langmuir		Modified Langmuir		
	RMSE	R^2	η_i	RMSE	R^2
Sc	3.344	0.8754	589.8	3.901	0.864
Y	91.75	-0.1699	8.41	35.36	0.861
	Extended Freundlich				
	x_i	y_i	z_i	RMSE	R^2
Sc	$-2*10^{-8}$	-30.13	61.23	0.0013	0.999
Y	$-7.38*10^{5}$	-172.9	193.8	0.0015	0.999
	Langmuir-Freundlich				

	a_i	m_i	m_j	b_i	b_j	RMSE	R^2
Sc	28.1	15.7	37.2	-0.3827	0.9395	0.3422	0.9997
Y	0.6948	0.4387	0.0344	0.3171	0.9502	439.8	-4.377

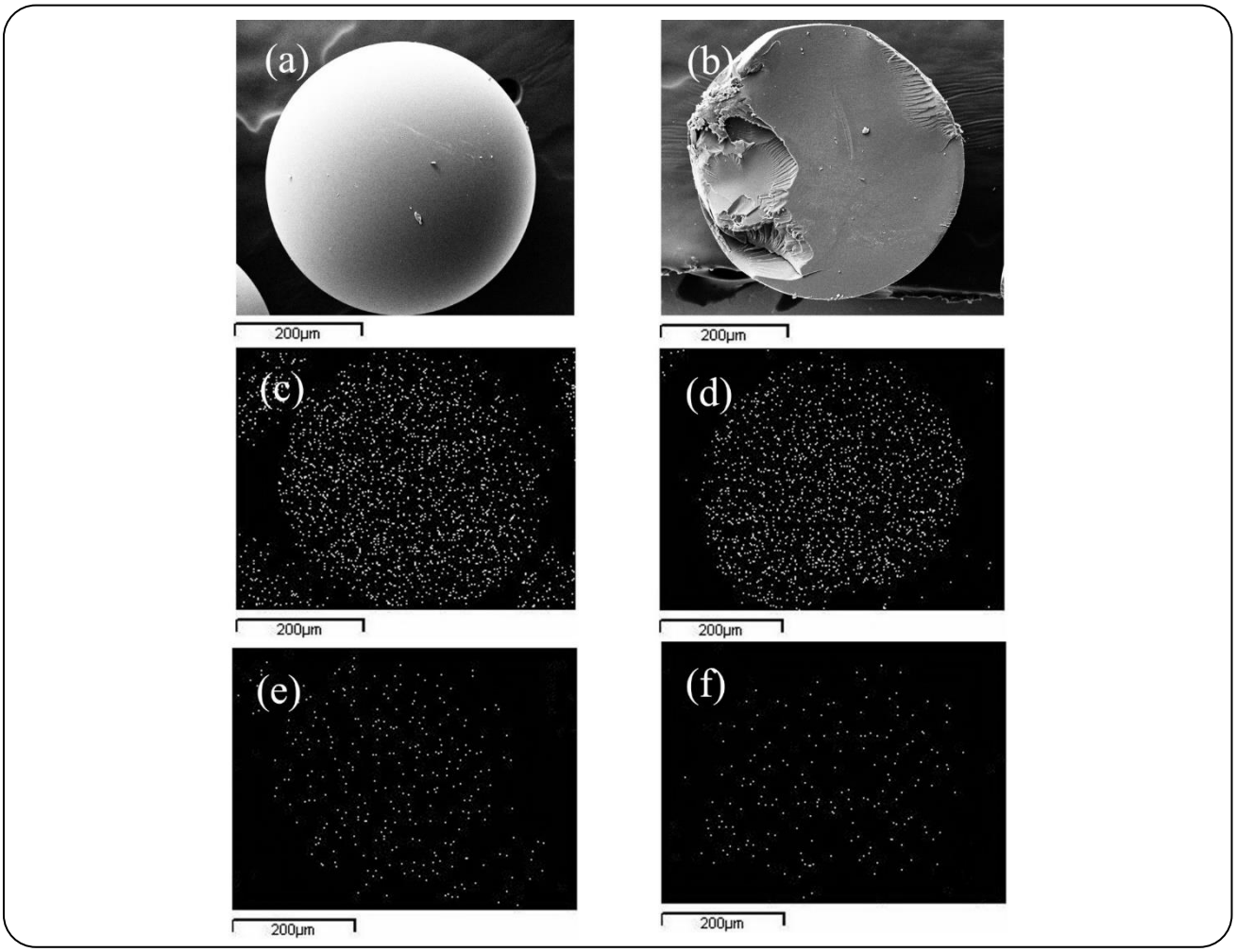

Fig. 2: FESEM pictures from Purolite resin beads following adsorption (a) outer surface; (b) cleavaged surface; (c,d) distribution map of adsorbed Sc from electrolyte carrying Sc alone; (e,f) distribution map of adsorbed Sc from an electrolyte containing Y and Sc.

diminishes the available sites for interacting with the Sc, giving the impression that Purolite C100 favors Y over Sc which is incorrect.

Adsorption Kinetic

Adsorption kinetics is important for adopting any adsorption system. Analysis of ion exchange kinetics such as rate-determining step, rate laws, and suitability of the ion exchange process is key to evaluating any system[42]. Essential parameters for Sc uptake from both single and binary systems have been appraised through Sc and Y sorption at different temperatures. Kinetics of static (batch) adsorption was modeled using a linear form of pseudo-first-order, pseudo-second-order, Elovich, and intra-particle diffusion equations (Eqs. (11–14)). [53]:

$$\text{Pseudo first} - \text{order equation}: \log(q_e - q_t) = \log q_e - \frac{K_1}{2.3}t \quad (11)$$

$$\text{Pseudo second} - \text{order equation}: \frac{t}{q_t} = \frac{1}{K_2 q_e^2} + \frac{1}{q_e}t \quad (12)$$

$$\text{Elovich equation}: q_t \frac{1}{\beta}\ln(\alpha\beta) + \frac{1}{\beta}\ln t \quad (13)$$

$$\text{Intra} - \text{particle diffusion equation}: q_t K_i t^{1/2} \quad (14)$$

Where q_t and q_e are the amounts of adsorbate (mg/g) at time (t) and at equilibrium respectively, k_1 the rate constant of pseudo first-order model (h^{-1}), k_2 the rate constant for pseudo-second-order (mg/g.h), α the initial sorption rate constant(mg/g.h), β is related to the extent of surface coverage and chemisorption energy of activation(mg/g) and k_i is the intra-particle diffusion rate constant ($mg/g.h^{½}$).

Kinetics of single and binary component adsorption

The calculated selectivity coefficients (R^2) for kinetics models as well as experimental results are summarized in Table 5 and Sc adsorption capacity based on the Langmuir isotherm is given in Table 3. Between all studied mechanisms, the second-order kinetic equation is more applicable. Based on experimental and calculated adsorption capacity values are relatively constant at around 100 mg/g, and it can be concluded that no significant difference exists between the continuous and batch systems. The measured capacity for Sc, found in this study is higher than other substances as quoted in literature (Table 6).

The q_e value for pseudo-second-order, single cation systems, is lower compared to the double ion solutions and proves the competitive interactions between Sc and Y ions which the overwhelming concentration of Y over Sc, retards Sc adsorption in their competition with Y-ions over adsorbent sites.

The generally accepted adsorption model for a bed of adsorbent, resin pearls are the Intraparticle Diffusion Model (IPM) through which rate-limiting step during the ion exchange process as well as the number of steps are determined [65]. The rate constants for Sc uptake for both systems corresponding to this model are shown in Figs. 3 and 4, in which the slope of each portion determines its rate [65]. The lower slope in binary adsorptions indicates a lower rate of absorption, due to the spatial constraints caused by the excess Y concentration over Sc ions.

According to this model absorption happens in three stages**:** First, diffusion of cations from the bulk solution to the layer surrounding the adsorbent, second, ion diffusion from this layer to the adsorbent surface and finally during stage 3, diffusion from the surface to the internal sites [50, 53, 66]. As shown in Figs 3 and 4, both in individual or binary ion solutions, Sc adsorption by Purolite C100 resin occurs in just two steps, as the third stage; i.e. diffusion from the surface to the internal sites and adsorption by the resin's functional groups are combined. This happens due to the gel makeup of the resin.

Comparing the slopes of each step in Figs. 3 and 4 show that the diffusion of the ions from the bulk solution to the adsorbent surrounding layer as the first step occurs at the highest rate, which is further accelerated by stirring the electrolyte at 130 rpm [58]. *Fathi et.al.* (2017) [58], studying the adsorption of Reusing microporous Purolite A170, and gel-type resin Dowex 21k, conclude that the adsorption steps reduce from three for the porous resin to two in the case of gel type. Similar to the present work, the slope of adsorption in the first stage is above the rest which they contributed to the stirring effect. The absence of the second phase observed in the present work is due to the gel structure of the Purolite C 100.

Table 5: Kinetic parameters of Sc adsorption on PuroliteC100 from single (Sc = 350 ppm) and binary (Sc = 100 ppm + Y = 500 ppm) system.

Model		Pseudo first-order				Pseudo second-order		
T (K)	System	q_e(exp)	q_e	K_1	R^2	q_e	K_2	R^2
		mg g^{-1}	mg g^{-1}	h^{-1}		mg g^{-1}	mg g^{-1} h^{-1}	
298	Single	101.02±0.48	6.48±2.40	0.0032±0.00	0.920	101.01±0.00	0.0033±0.00	0.999
	Binary	23.75±0.35	1.66±0.76	0.0028±0.00	0.861	23.58±0.51	0.0002±0.00	1
308	Single	99±0.42	7.09±2.00	0.0036±0.00	0.972	99.01±0.00	0.0032±0.00	1
	Binary	23.35±0.38	1.68±0.56	0.0028±0.00	0.851	23.15±0.58	0.0002±0.00	1
318	Single	97.5±0.43	7.44±1.97	0.0029±0.00	0.968	97.088±0.00	0.0028±0.00	0.999
	Binary	22.75±0.23	1.69±0.53	0.0031±0.00	0.913	22.62±0.31	0.0001±0.00	1
328	Single	92±0.30	5±2.12	0.0052±0.00	0.952	91.74±0.00	0.0055±0.00	1
	Binary	22.05±0.35	1.80±0.36	0.0045±0.00	0.956	22.05±0.43	0.0001±0.00	1
Model		Elovich				Intraparticle diffusion		
T (K)	System	α	β		R^2	K_i		R^2
		mg g^{-1} h^{-1}	mg g^{-1}			mg g^{-1} $h^{-0.5}$		
298	Single	246.87±1.68	0.697±0.04		0.973	0.243±0.00		0.879
	Binary	54.90±0.45	1.918±0.15		0.948	0.083±0.00		0.758
308	Single	243.06±1.26	0.620±0.05		0.996	0.277±0.00		0.924
	Binary	53.44±0.64	1.839±0.12		0.947	0.086±0.00		0.758
318	Single	231.63±2.11	0.595±0.02		0.991	0.289±0.00		0.922
	Binary	52.16±0.71	1.888±0.09		0.951	0.085±0.00		0.767
328	Single	181.71±1.50	0.798±0.05		0.962	0.204±0.00		0.800
	Binary	50.78±0.15	1.951±0.16		0.967	0.083±0.00		0.799

Table 6: The capacity for Sc ion adsorption with various adsorbents as reported in the literature.

Adsorbents	Isotherm Models	Kinetic Models	Maximum Adsorption Capacity (mg g^{-1})	References	Year
Lysine-Functionalized Mesoporous Material	F	Ps2	30.51	[62]	2014
SiO_2-[A336][L]	L	Ps2	0.27	[63]	2016
Tulsion CH 93 Resin	-----	-----	22.00	[36]	2017
Purolite D 5041 Resin	-----	-----	20.00	[36]	2017
Pine Wood Sawdust (SD)	F	Ps2	7.50	[64]	2017
Activated Carbon (AC)	F	Ps2	8.50	[64]	2017
Activated Carbon (AC)	-----	Ps1	10.11	[17]	2018
TP 260 Resin	-----	Ps2	66.23	[48]	2018
TP 209 Resin	-----	Ps2	22.47	[48]	2018
TP 272 Resin	-----	Ps2	11.29	[48]	2018
Purolite C 100	F	Ps2	101.02	(this work)	2020

L-Langmuir; F-Freundlich;Ps1-Pseudo first order kinetic model; Ps2-Pseudo second order kinetic model.

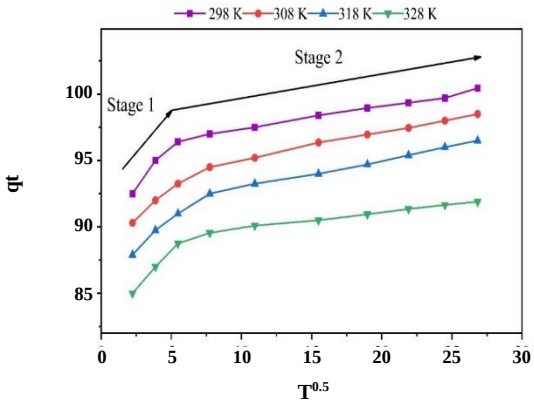

Fig. 3: Intra-particle diffusion equation for the adsorption of Sc from single system on the C100 resin at the different temperature. Initial concentration of metal ions = 350 mg/L, resin dosage = 0.1 mg, pH =1.5.

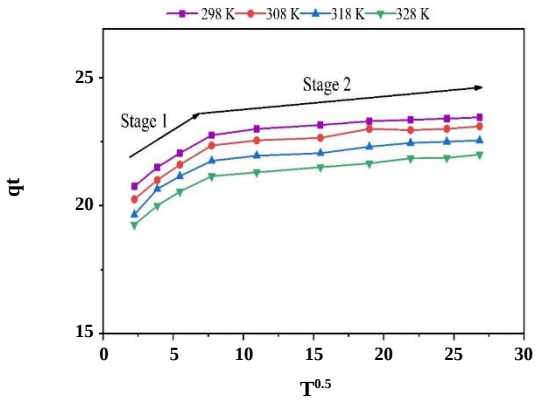

Fig. 4: intra-particle diffusion plots for the adsorption of Sc from binary (Sc-Y) system on the Purolite C100 resin at different temperatures. The initial concentration of metal ions Sc = 100 mg/L, Y= 500 mg/L resin dosage = 0.1 mg, pH = 1.5.

Adsorption thermodynamics

To ascertain the impact of Sc & Y adsorption on thermodynamics of the system, changes in the standard enthalpy (ΔH°), standard entropy (ΔS°) and standard free energy (ΔG°) with temperature were calculated using the following equations:

$$K_{ad} = \frac{C_a}{C_e} \tag{15}$$

$$\Delta G^{\circ} = -RT \ln K_{ad} \tag{16}$$

$$\Delta G^{\circ} = \Delta H^{\circ} - T\Delta S^{\circ} \tag{17}$$

$$\ln K_{ad} = \frac{\Delta S^{\circ}}{R} - \frac{1}{T}\frac{\Delta H^{\circ}}{R} \tag{18}$$

where R is the gas constant, T, the reaction temperature (K), K_{ad}, adsorption equilibrium constant, C_a and C_e are the concentration of Sc on the adsorbent and solution at equilibrium (mg/L) respectively. ΔH can be calculated from the slope of $\ln K_{ad}$ versus (1/T) according to Eq. (19) the Van't Hoff plot [67, 68]. Table 7 shows thermodynamic data for Sc adsorption individually and in Sc-Y binary system. The negative value of ΔH° in either system shows the dissipation of energy to the environment and the exothermic nature of such adsorption [69]. Reduced absorption efficiency under ion competition for adsorbent sites can also be deduced from the enthalpies of the two systems as shown in Table 7. Reduction in the number of bonds between functional groups in the resin and Sc ions reduces the amount of dissipated heat.

The negative enthalpy values of (-5.97 kJ./mol) for Sc adsorption from double ion solutions and (-5.38 kJ./mol) when it is absorbed from a single ion medium (Table 7) show energy is given off which is indicative of exothermic adsorption [69]. In fact the more negative value for the competitive adsorption from double ion solutions attests to the lowered interaction and weaker bonding which could be misconstrued as less efficient adsorption if the five-fold prevalence of yttrium is overlooked. Taking these values in to account, in the competitive two-element system, the fall in bond numbers between the functional groups of the resin and Sc because of the Y interactions, reduces the heat given off. This argument has been put forward by other researchers when describing the drop in heat dissipated from adsorption of rhenium from Re-Mo system on Purolite A170 compared to its adsorption singly [50].

The variations of Gibbs free energies (ΔG°), for cation adsorption on Purolite in both investigated systems in Table 7, show that higher temperatures induce a ΔG° rise confirming that, at elevated temperatures, the absorption diminishes [70, 71], so lower temperatures are more favorable.

Generally, ΔS° value is an indication of whether the reaction follows an associative or a dissociative mechanism. A ΔS° value greater than −10 J/mol.K implies a dissociative mechanism, whereas a high negative value much less than −10 $J.mol^{-1}.K^{-1}$ indicates an

Table 7: Thermodynamic parameters of Sc adsorption onto the Purolite C100 from single (Sc = 350 ppm) and binary (Sc = 100 ppm – Y = 500 ppm) system.

System	Δ H (kJ/mol)	ΔS (J/mol K)	ΔG (kJ/mol)			
			T = 298 K	T = 308 K	T = 318 K	T = 328 K
Single	-5.97±0.14	-15.56±0.31	-1.31	-1.17	-1.02	-0.86
Binary	-5.38±0.09	-16±0.24	-0.61	-0.45	-0.29	-0.13

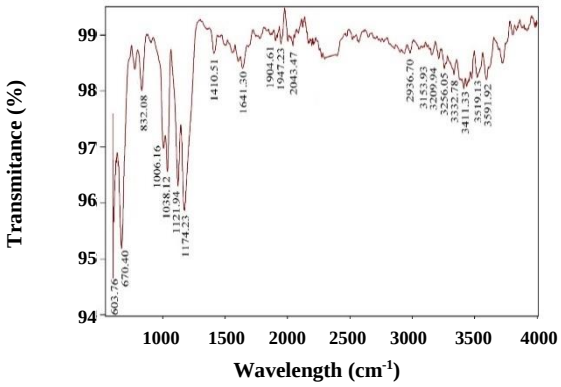

Fig. 5: FTIR diagram of Primary Purolite C100 Resin.

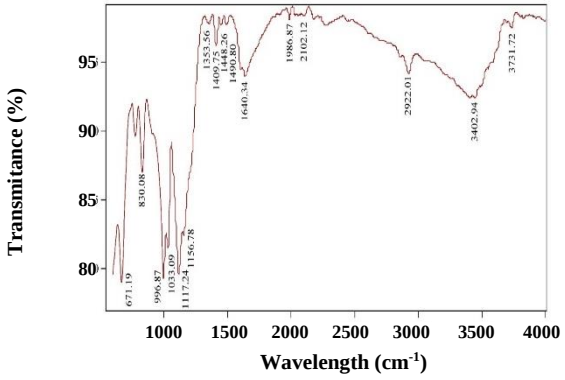

Fig. 6: FT-IR diagram of Purolite C100 Resin after absorption of Sc.

associative mechanism [72]. According to Table 7, entropy for adsorption of cations either from single or binary ion-carrying electrolytes is less than -10 J/mol.K, indicating an associative mechanism. The more negative entropy for adsorption in this binary system is due to competing ions, making free access to adsorption sites more difficult hence reducing the amount of ion exchange.

FT-IR analysis results

As Fig. 5 shows, the C-S bond between the polymeric carbon functional group of the resin and the stable part of the polymer i.e. SO_3 with peaks in the 600-700 cm^{-1} range. The 832.08 cm^{-1} peak represents the attachment of the benzene ring of the divinylbenzene to sulfonic ion. The 1121.94, 1038.12, 1174.23 cm^{-1} all belong to the sulfonic group whose S=O bond occurs at 1410.51 peak. C-H bond peak of the styrene ring is shown at 1600 cm^{-1} and the C=C=C within the 1900-2100 cm^{-1} domain. So the 2936.70-3153.93 cm^{-1} range represents the polystyrene structure with the usual 3200-3600 cm^{-1} demonstrating the hydroxyl ion functional group [73].

Fig. 6, shows the FTIR fingerprint for Purolite structure following Sc adsorption on it. Evidently, the 1300 cm^{-1} peak which corresponds to Sc is absent in the previous figure while a singular 1353.56 cm^{-1} peak representing the Sc-O boning [74] is detectable and proves successful adsorption of Sc on Purolite.

Fig. 7, demonstrates the FT-IR analysis of Sc adsorption in presence of yttrium confirming its adsorption as the above peak is observed but with a slight displacement to 1353.80 cm^{-1}. The 1000 cm^{-1} range displays the Y presence on the adsorbate [75].

Sc extraction from the actual copper leach solution

Thermodynamic studies indicated an inverse relationship between adsorption and temperature so these tests were carried out at room temperature by passing the solution through a column containing the adsorbent. Results shown in Fig. 8 demonstrate successful extraction of Sc with total saturation happening at 450 BV with one BV equal to 20 mL.

These columns were then eluted with 6M HNO_3 and as Fig. 9 shows, the Sc-peak during desorption occurred at 9 BV after Y-peak. This tallies well with the adsorption isotherm results as the values of K_l in the Langmuir,

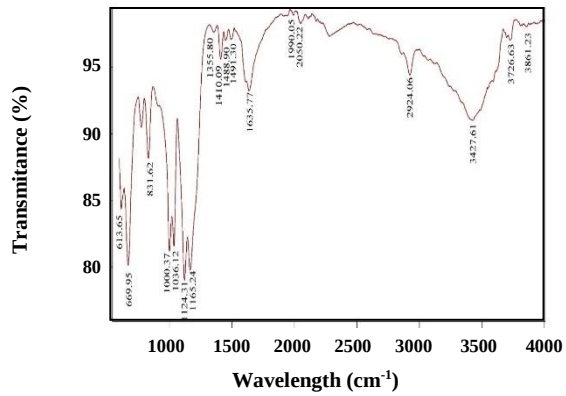

Fig. 7: FTIR diagram of Purolite C100 Resin after absorption of Sc and Y.

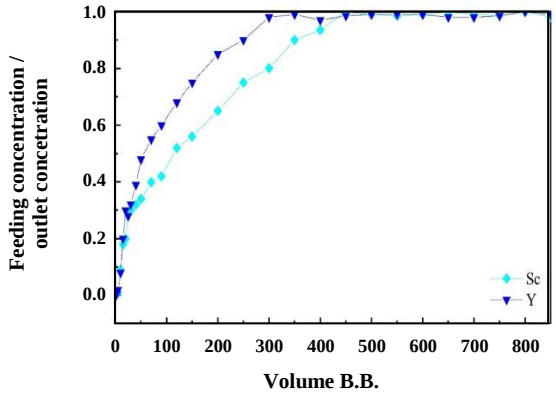

Fig. 8: Adsorption Curves of Sc and Y on Purolite C100 Resin from the actual copper leach solution.

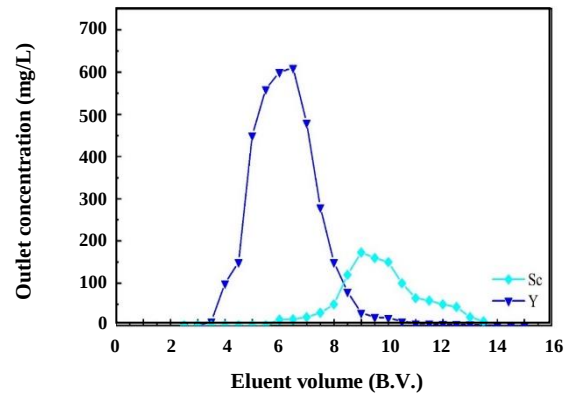

Fig. 9: Eluting Curves of Sc and Y from the Purolite C100 Resin by HNO_3 (6M) Solution.

b in Temkin and E in the Dubinin-Radushkevich are all higher for Sc as compared to yttrium and confirm that Sc is much more strongly adsorbed by Purolite and despite the excess concentration of Y, this preference for scandium is clear and thus, it is washed away later. The final solution following the extraction procedure was a scandium-rich one with 180 mg/L concentrate corresponding to a 60:1 single step increase in the concentration of scandium.

CONCLUSIONS

The adsorption mechanism for scandium on Purolite C100Na either alone or in conjunction with Y-ions was studied through adsorption isotherms, kinetics, and thermodynamic modeling.

Both Scandium and Yttrium when adsorbed from an electrolyte that carries either one individually follow the Freundlich isotherm and the value of (n) show the absorption medium is appropriate for both. Sc adsorption from an electrolyte carrying Sc-Y, is defined well by the Langmuir-Freundlich isotherm. Kinetics studies showed that the adsorption of these ions, individually or combined, follows a second-order kinetic model and as Table 5 shows with a high correspondence demonstrated by an R^2 value greater than 0.999. The process mechanism is explained by Intraparticle Diffusion Model (IDM), whether adsorption occurs from single or double ion solutions. It was found that due to the gel-like form of this adsorbent, Sc absorption by resin happens in just two steps as the third step i.e. absorption of cation by the functional groups of adsorbent is combined with the diffusion from the surface to the internal sites.

The negative value of $\Delta H°$ in either one of single (-5.97 kJ/mol) or binary (-5.38 kJ/mol) ion systems shows the adsorption process gives off energy and the reaction, therefore, is exothermic. Diminished efficiency of Sc adsorption by the Purolite under the competing condition which happens in presence of yttrium, causes a fewer number of bonds between resin functional groups and Sc ions leading to reduced heat dissipation by the system as is noticed from the results.

The variations in ($\Delta G°$) with temperature for both systems show that at higher temperatures, $\Delta G°$ becomes more positive i.e. the absorption is restricted. Adsorption process by Purolite C100Na from single or binary ion solutions show entropy values of around -10 mol^{-1} K^{-1}, indicating an associative mechanism, however, it is slightly

more negative in the binary state due to ions competing for a set number of sites. The high ratio of Y:Sc found in the actual mine test solutions makes Scandium's access more difficult and reduces the amount adsorbed. In order to confirm the adsorption characteristics of this resin, its FT-IR analysis was compared before and after the adsorption process both in single and double ion tests. The results on the extracted leach solution from the actual mine showed excellent selectivity for Sc despite the presence of copper, Y and a host of other cations in the electrolyte Elution studies also confirmed the theoretical appraisal with desorption peak for Sc occurring way after that of yttrium. The final one-step adsorption/elution process resulted in a Sc rich 180 mg/L solution indicative of 60:1 increased concentration.

Acknowledgments

The authors gratefully acknowledge financial support from the National Iranian Copper Industries Co. (NICICO).

Received : Nov. 11, 2019 ; Accepted : May 4, 2020

REFERENCES

[1] Krishnamurthy N., Gupta CK., "Extractive Metallurgy of Rare Earths", CRC Press (2015).

[2] Van Nguyen N., Iizuka A, Shibata E., Nakamura T., "Recovery of Scandium from Chloride Media Using the Novel Ion Exchange Resin", *Proceedings of the World Congress on Mechanical, Chemical, and Material Engineering*. Barcelona, Spain ., 3381-3384 (2015).

[3] Zemlyanoy S., Gangrsky Y., Marinova K., Avgoulea M., Billowes J., Campbell P., Cheal B., Tordoff B., Fritzsche S., Loblonskyi D., Barbieri C., Simpson E.C., Sterenson P.D., Bissell M.L., Forest D.H., Gardner M.D., Tungate G., Huikari J., Nieminen A., Penttila H., "Nuclear Charge Radii and Electromagnetic Moments of Scandium Isotopes and Isomers", *Proceedings of the 8th Conference on Nuclear and Particle Physics*, Hurghada, Egyp., 27-28 (2011).

[4] Kim J., Azimi G., "An Innovative Process for Extracting Scandium from Nickeliferous Laterite Ore", Rare Metal Technology 2020, Springer (2020).

[5] Badwal S., Ciacchi F., Milosevic D., Scandia–Zirconia Electrolytes for Intermediate Temperature Solid Oxide Fuel Cell Operation, *Solid. State. Ion.*, **136**: 91-9 (2000).

[6] Thapa R., Nissinen T., Turhanen P., Määttä J., Vepsäläinen J., Lehto V-P., Riikonen J., Bisphosphonate Modified Mesoporous Silicon for Scandium Adsorption, *Microporous. Microporous. Mater.*, **296**:109980 (2020).

[7] Altinsel Y., Topkaya Y., Kaya Ş., Şentürk B., "Extraction of Scandium from Lateritic Nickel-Cobalt ore Leach Solution by Ion Exchange: A Special Study and Literature Review on Previous Works," TMS Annual Meeting & Exhibition, Springer., 1545-1553 (2018).

[8] Zhang N., Li H-X., Liu X-M., Recovery of Scandium from Bauxite Residue—Red Mud: A Review, *Rare. Metals.*, **5**:887-900 (2016).

[9] Zhang Y., Zhao H., Sun M., Zhang Y., Meng X., Zhang L., Lv X., Davaasambuu S., Qiu G., Scandium Extraction from Silicates by Hydrometallurgical Process at Normal Pressure and Temperature, *J. Mater. Res. Technol.*, **9**: 709-17 (2020).

[10] Wang W., Cheng C.Y., Separation and Purification of Scandium by Solvent Extraction and Related Technologies: A Review, *J. Chem. Technol. Biotechnol.*, **86**:1237-46 (2011).

[11] Wang W., Pranolo Y., Cheng C.Y., Metallurgical Processes for Scandium Recovery from Various Resources: A Review, *Hydrometallurgy.*, **108**:100-108 (2011).

[12] Habashi F., "A textbook of hydrometallurgy", Métallurgie Extractive (1999).

[13] Ross J., Rosenbaum J., "Reconnaissance of Scandium Sources and Recovery of Scandium from Uranium Mill Solutions: US Dept of Interior", US Dept. of Interior, Bureau of Mines (1962).

[14] Nebeker N., Hiskey J.B., Recovery of Rhenium from Copper Leach Solution by Ion Exchange, *Hydrometallurgy.*, **125**:64-68 (2012).

[15] Hiskey J.B., Copp R.G., Recovery of Yttrium and Neodymium from Copper Pregnant Leach Solutions by Solvent Extraction, *Hydrometallurgy.*, **177**:21-26 (2018).

[16] Felipe E., Batista K., Ladeira A., Recovery of Rare Earth Elements from Acid Mine Drainage by Ion Exchange, *Environ. Technol.*, 1-32 (2020).

[17] Burakova I., Burakov A., Tkachev A., Troshkina I., Veselova O., Babkin A.V., Moe Aung W., Ali I., Kinetics of the Adsorption of Scandium and Cerium Ions in Sulfuric Acid Solutions on a Nanomodified Activated Carbon, *J. Mol. Liq.*, **253**:277-283 (2018).

[18] Torab-Mostaedi M., Asadollahzadeh M., Hemmati A., Khosravi A., Biosorption of Lanthanum and Cerium From Aqueous Solutions by Grapefruit Peel: Equilibrium, Kinetic and Thermodynamic Studies, *Res. Chem. Intermed.*, **41**: 559-73 (2015).

[19] Varshini C., Nilanjana D.n., Screening of Biowaste Materials for the Sorption of Cerium (III) from Aqueous Environment, *Res. J. Pharm., Bi*ol. *Chem. Sci.*, **5**: 402-408 (2014).

[20] Yao T., Xiao Y., Wu X., Guo C., Zhao Y., Chen X., Adsorption of Eu (III) on Sulfonated Graphene Oxide: Combined Macroscopic and Modeling Techniques, *J. Mol. Liq.*, **215**:443-8 (2016).

[21] Das D., Varshini CJS., Das N., Recovery of Lanthanum (III) from Aqueous Solution Using Biosorbents of Plant and Animal Origin: Batch and Column Studies, *Miner. Eng.*, **69**:40-56 (2014).

[22] Butnariu M., Negrea P., Lupa L., Ciopec M., Negrea A., Pentea M., Sarac L., Samfira L., Remediation of Rare Earth Element Pollutants by Sorption Process Using Organic Natural Sorbents, *Int. j. Environ. Res. Public Health.*, **12**: 11278-11287 (2015).

[23] Dubey S.S., Grandhi S., Sorption Studies of Yttrium (III) Ions on Nano Maghemite, *J. Environ. Chem. Eng.*, **4**: 4719-30 (2016).

[24] Ogata T., Narita H., Tanaka M., Adsorption Behavior of Rare Earth Elements on Silica Gel Modified with Diglycol Amic Acid, *Hydrometallurgy.*, **152**:178-182 (2015).

[25] Karamzadeh Z., Yaftian M.R., Shiri Yekta Z., Nilchi A., Dolatyari L., Extraction-Separation of Eu (III)/Th (IV) Ions with a Phosphorylated Ligand in an Ionic Liquid, *Iran. J. Chem. Chem. Eng. (IJCCE)*, **35(2)**: 89-95 (2016).

[26] Ola P.D., Matsumoto M., "Metal Extraction with Ionic Liquids-Based Aqueous Two-Phase System", Recent Advances in Ionic Liquids (2018).

[27] Han D., Row K.H., Recent Applications of Ionic Liquids in Separation Technology, *Molecules.*, **15**: 2405-2426 (2015).

[28] Kumar S., Jain S., History, introduction, and Kinetics of Ion Exchange Materials, *J. Chem.*, **2013**:1-13 (2013).

[29] Page M.J, Soldenhoff K, Ogden M.D., Comparative Study of the Application of Chelating Resins for Rare Earth Recovery, *Hydrometallurgy.*, **169**:275-281 (2017).

[30] Ochsenkühn-Petropoulou M.T., Hatzilyberis K.S., Mendrinos L.N., Salmas C.E., Pilot-Plant Investigation of the Leaching Process for the Recovery of Scandium from Red Mud, *Ind. Eng. Chem. Res.*, **41**:5794-801 (2002).

[31] Chao H-E., Suzuki N., Adsorption Behaviour of Scandium, Yttrium, Cerium and Uranium from Xylenol Orange Solutions onto Anionexchange Resins, *Anal. Chim. Acta.*, **125**:139-47 (1981).

[32] Faris J., Warton J., Anion Exchange Resin Separation of the Rare Earths, Yttrium, and Scandium in Nitric Acid-Methanol Mixtures, *Anal. Chem.*, **34**:1077-1080 (1981).

[33] Wang W., Pranolo Y., Cheng C.Y., Recovery of Scandium from Synthetic Red Mud Leach Solutions by Solvent Extraction with D2EHPA, *Sep. Purif. Technol.*, **108**:96-102 (2013).

[34] Rychkov V.N., Semenishchev V.S., Mashkovtsev M.A., Kirillov E.V., Kirillov S.V., Bunkov GM., Botalov M.S., Deactivation of the Scandium Concentrate Recovered from Uranium Leach Liquors, *J. Radioanal. Nucl. Chem.*, **310**:1247-53, (2016).

[35] Wakui Y, Matsunaga H, Suzuki TM., Sective Recovery of Trace Scandium from Acid Aqueous Solution with (2-ethylhexyl hydrogen 2-ethylhexylphosphonate)-Impregnated resin, *Anal. sci.*, **5**:189-93 (1989).

[36] Smirnov A.L., Titova S.M., Rychkov V.N., Bunkleov G.M., Semenishchev V.S, Kirillov E.V, Poponin N.B., Svirsky I.A.. Study of Scandium and Thorium Sorption from Uranium Leach Liquors, *J. Radioanal. Nucl. Chem.*, **312**:277-283 (2017).

[37] Broekaert J., Hörmann P., Separation of Yttrium and Rare Earth Elements from Geological Materials, *Anal. Chim. Acta.*, **124**:421-5 (1981).

[38] Koopman C, Witkamp G, Van Rosmalen G., Removal of Heavy Metals and Lanthanides from Industrial Phosphoric Acid Process Liquors, *Sep. Sci. Technol.*, **34**:2997-3008 (1999).

[39] Chour Z., Laubie B., Morel JL., Tang Y., Qiu R., Simonnot M-O., Muhr L., Recovery of Rare Earth Elements from Dicranopteris Dichotoma by an Enhanced Ion Exchange Leaching Process, *Chem. Eng. Process.*, **130**:208-213 (2018).

[40] Zinovyev V.G., Mitropolsky I.A., Shulyak G.I., Sushkov P.A., Tyukavina T.M., Sakharov S.L., Malyutenkov E.I., Tikhonova A.E., Okunev I.S., Study of the Gadolinium Sorption on the C100 Ion-Exchange Resin for the Development of the Antineutrino Detector Targets, *J. Radioanal. Nucl. Chem.*, **315**: 459-473 (2018).

[41] Abo-Farha S., Abdel-Aal A., Ashour I., Garamon S., Removal of Some Heavy Metal Cations by Synthetic Resin Purolite C100, *J. Hazard. Mater.*, **169**:190-4 (2009).

[42] Khan MDA., Akhtar A., Nabi S.A., Kinetics and Thermodynamics of Alkaline Earth and Heavy Metal Ion Exchange under Particle Diffusion Controlled Phenomenon Using Polyaniline-Sn (Iv) Iodophosphate Nanocomposite, *J . Chem. Eng. Data.*, **59**:2677-2685 (2014).

[43] Fathi M.B., Rezai B., Keshavarz Alamdari E., Alorro R.D., Equilibrium Modeling In Adsorption of Re and Mo Ions from Single and Binary Aqueous Solutions on Dowex 21K Resin, Geosyst. *Eng.*, **21**:73-80 (2018).

[44] Salarirad MM., Behnamfard A., "Modeling of Equilibrium Data for Free Cyanide Adsorption onto Activated Carbon by Linear and Non-Linear Regression Methods", International Conference on Environment and Industrial Innovation, 79-84 (2011).

[45] Samadani Langeroodi N, Farhadravesh Z, Dehno Khalaji A., Optimization of Adsorption Parameters for Fe (III) Ions Removal from Aqueous Solutions by Transition Metal Oxide Nanocomposite, *Green. Chem. Lett. Rev.*, **11**:404-413 (2018).

[46] Safaei E., Langeroodi N.S., Baher E., Investigation of Removal of Cu (II) Ions by Commercial Activated Carbon: Equilibrium and Thermodynamic Studies, *Pro. Met. Phys. Chem. Surf.*, **55**:28-33 (2019).

[47] Tajari E., Langeroodi N.S., Khalafi M., Statistical Modeling, Optimization and Kinetics of Mn2+ Adsorption in Aqueous Solution Using a Biosorbent, *Z. Phys. Chem.*, **233**:1201-1214 (2019).

[48] Bao S., Hawker W., Vaughan J., Scandium Loading on Chelating and Solvent Impregnated Resin from Sulfate Solution, *Solvent Extr. Ion Exch.*, **36**:100-113 (2018).

[49] Ochsenkühn-Petropulu M., Lyberopulu T., Parissakis G., Selective Separation and Determination of Scandium from Yttrium and Lanthanides in Red Mud by a Combined Ion Exchange/Solvent Extraction Method, *Anal. Chim. Acta.*, **315**:231-237 (1995).

[50] Fathi MB., Rezai B., Alamdari E.K., Competitive Adsorption Characteristics of Rhenium in Single and Binary (Re-Mo) Systems Using Purolite A170, *Int. J. Miner. Process.*, **169**:1-6 (2017).

[51] Shahmohammadi-Kalalagh S., Isotherm and Kinetic Studies on Adsorption Of Pb, Zn and Cu by Kaolinite, *Casp. J. Environ. Sci.*, **9**:243-255 (2011).

[52] Ba S., Ennaciri K., Yaacoubi A., Alagui A., Bacaoui A., Activated Carbon from Olive Wastes as an Adsorbent for Chromium Ions Removal, *Iran. J. Chem. Chem .Eng. (IJCCE)*, **37(6)**:107-123 (2018).

[53] Lou Z., Zhao Z., Li Y, Shan W., Xiong Y., Fang D., Yue Sh., Zang Sh., Contribution of Tertiary Amino Groups to Re (VII) Biosorption on Modified Corn Stalk: Competitiveness and Regularity, *Bioresour. Technol.*, **133**: 546-554 (2013).

[54] Dada A., Olalekan A., Olatunya A., Dada O., Langmuir, Freundlich, Temkin and Dubinin–Radushkevich Isotherms Studies of Equilibrium Sorption of Zn^{2+} unto Phosphoric Acid Modified Rice Husk, *IOSR. J. Appl. Chem.*, **3(1)**:38-45 (2012).

[55] Günay A., Arslankaya E., Tosun I., Lead Removal from Aqueous Solution by Natural and Pretreated Clinoptilolite: Adsorption Equilibrium and Kinetics, *J. Hazard. Mater.*, **146**:362-371 (2007).

[56] Liu J., Wang X., Novel Silica-Based Hybrid Adsorbents: Lead (II) Adsorption Isotherms, *Sci. World J.*, **2013**: 362 – 371 (2013).

[57] Singha B., Das S.K., Adsorptive Removal of Cu (II) from Aqueous Solution and Industrial Effluent Using Natural/Agricultural Wastes, *Colloids Surface. B.*, **107**:97-106 (2013).

[58] Fathi M., Rezai B., Alamdari E., Alorro R., Studying Effects of Ion Exchange Resin Structure and Functional Groups on Re (VII) Adsorption onto Purolite A170 and Dowex 21K, *J. Min. Reclam. Environ.*, **9**:243-254 (2018).

[59] Treybal RE., "Mass Transfer Operations", McGraw-Hill Book Co., New York 466 (1973).

[60] Zhu Y, Hu J, Wang J., Competitive Adsorption of Pb (II), Cu (II) and Zn (II) onto Xanthate-Modified Magnetic Chitosan, *J. Hazard. Mater.*, **221**:155-161 (2012).

[61] Mahamadi C., Nharingo T., Competitive Adsorption of Pb^{2+}, Cd^{2+} and Zn^{2+} Ions onto Eichhornia Crassipes in Binary and Ternary Systems, *Bioresour. Technol.*, **101**:859-864 (2010).

[62] Ma J., Wang Z., Shi Y., Li Q., Synthesis and Characterization of Lysine-Modified SBA-15 and Its Selective Adsorption of Scandium from a Solution of Rare Earth Elements, *RSC. Adv.*, **4**: 41597-41604 (2014).

[63] Turanov A.N., Karandashev V.K., Sukhinina N.S., Masalov V.M., Emelchenko G.A., Adsorption of Lanthanides and Scandium Ions by Silica Sol-Gel Material Doped with Novel Bifunctional Ionic Liquid, Trioctylmethylammonium 1-Phenyl-3-Methyl-4-Benzoyl-5-Onate, *J. Environ. Chem. Eng.*, **4**:3788-3796 (2016).

[64] Komnitsas K., Zaharaki D., Bartzas G., Alevizos G., Adsorption of Scandium and Neodymium on Biochar Derived after Low-Temperature Pyrolysis of Sawdust, *Minerals.*, **7**: 200 (2017).

[65] Wu F-C., Tseng R-L., Juang R-S., Initial Behavior of Intraparticle Diffusion Model Used in the Description of Adsorption Kinetics, *Chem. Eng. J.*, **153**:1-8 (2009).

[66] Igwe J., Abia A., A Bioseparation Process for Removing Heavy Metals from Waste Water Using Biosorbents, *Afr. J. Biotechnol.*, **5**: (2006).

[67] Xu Z., Han D., Li Y., Zhang P., You L., Zhao Z., High Removal Performance of a Magnetic FPA90-Cl Anion Resin for Bromate and Coexisting Precursors: Kinetics, Thermodynamics, and Equilibrium Studies, *Environ. Sci. Pollut. Res.*, 1-14 (2018).

[68] Djawad F., Djamel N., Elhadj M., Samira A., Adsorption of Ni2+ Ions onto NaX and NaY Zeolites: Equilibrium, Kinetic, Intra Crystalline Diffusion and Thermodynamic Studies, *Iran. J. Chem. Chem. Eng. (IJCCE)*, **38(6)**: 63-81 (2018).

[69] Khawassek Y., Masoud A., Taha M., Hussein A., Kinetics and Thermodynamics of Uranium Ion Adsorption from Waste Solution Using Amberjet 1200 H as Cation Exchanger, *J. Radioanal. Nucl. Chem.*, **315**:493-502 (2018).

[70] Fil BA., Boncukcuoğlu R., Yilmaz AE., Bayar S., Adsorption of Ni (II) on Ion Exchange Resin: Kinetics, Equilibrium and Thermodynamic Studies, *Korean J . Chem. Eng.*, **29**:1232-1238 (2012).

[71] Gorimbo J., Taenzana B., Kapanji K., Jewell L.L., Equilibrium Ion Exchange Studies of Ni2+ on homoionic Forms of Clinoptilo, *S. Afr. J. Sci.*, **110**: 01-7 (2014).

[72] El-Naggar I., Zakaria E., Ali I., Khalil M., El-Shahat M., Kinetic Modeling Analysis for the Removal of Cesium Ions from Aqueous Solutions Using Polyaniline Titanotungstate, *Arabian. J. Chem.*, **5**: 109-119 (2012).

[73] Lazar L., Bandrabur B., Tataru-Fărmuş R-E., Drobotă M., Bulgariu L., Gutt G., FTIR Analysis of Ion Exchange Resins with Application In Permanent Hard Water Softening, *Environ. Eng. Manage. J. (EEMJ)*, **13(9)**: (2014).

[74] Liu J., Yang X., Cheng X., Peng Y., Chen H., Synthesis and Application of Ion-Imprinted Polymer Particles for Solid-Phase Extraction and Determination of Trace Scandium by ICP-MS in Different Matrices, *Anal. Methods.*, **5**:1811-1817 (2013).

[75] Sheibley D.W., Fowler M.H., "Infrared Spectra of Various Metal Oxides the Region of 2 to 26 Microns", National Aeronautics and Space Administration, Cleveland, Ohio. Lewis Research Center (1966).